Korean J. Chem. Eng., 32(4), 767-776 (2015)
DOI: 10.1007/s11814-014-0251-8

pISSN: 0256-1115
eISSN: 1975-7220

Preparation and characterization of molecularly-imprinted magnetic microspheres for adsorption of 2,4,6-trichlorophenol from aqueous solutions

Ping Yu*,, Qilong Sun***, Jianfeng Li****, Zhenjiang Tan**,†, Jianming Pan*, and Yongsheng Yan*,†**

*School of Chemistry and Chemical Engineering, Jiangsu University, Zhenjiang 212013, China
**School of Computer Science, Jilin Normal University, 1301 Haifeng Street, Siping 136000, China
***School of Management, Jilin Normal University, 1301 Haifeng Street, Siping 136000, China
****School of Foreign language, Jilin Normal University, 1301 Haifeng Street, Siping 136000, China
(*Received 15 June 2014 • accepted 26 August 2014*)

Abstract−Magnetic molecularly imprinted microspheres (MMIS) were successfully prepared by suspension polymerization, and then as-prepared MMIS were used as adsorbents for selective recognition of 2,4,6-trichlorophenol (2,4,6-TCP) from aqueous solutions. The results composites were characterized by Fourier transform infrared (FT-IR), X-ray diffraction (XRD), thermo gravimetric analysis (TGA), scanning electron microscope (SEM) and vibrating sample magnetometer (VSM). The results demonstrated that MMIS possesses porous spherical morphology, and exhibits good thermal stability and magnetic property (Ms=10.14 emu g^{-1}). Then batch mode of binding experiments was used to determine the equilibrium, kinetics and selectivity recognition. The Langmuir isotherm model fitted the equilibrium data better than did the Freundlich model, and the maximum adsorption capacity on MMIS was about 1.7 times higher than that of MNIS. Kinetics behaviors of MMIS were well described by the pseudo-second-order model. MMIS possessed outstanding selectivity recognition for 2,4,6-TCP in the presence of other competitive phenols (such as sesamol, 3-CP, thymol, 2,4-DCP). Furthermore, the reusability performance of MMIS showed about 17.53% loss after five repeated cycles. Finally, the MMIS were successfully applied to the selective extraction of 2,4,6-TCP from the vegetable samples.

Keywords: Suspension Polymerization, Molecularly Imprinted Microspheres, Magnetic, 2,4,6-Trichlorophenol, Selective Recognition

INTRODUCTION

Chlorophenols and derivatives, such as 2,4,6-trichlorophenol (2,4,6-TCP), are extensively used as chemical raw materials, such as petroleum refineries, chemicals, plastic, rubber, tanning, steel plants, pharmaceuticals, disinfectant, wood, paper photographic and dye [1]. As the main ingredient of pesticides and herbicides, chlorophenols are widely used in industrial and agricultural production. At the same time, they have been listed as priority pollutants by the Environmental Protection Agency (EPA) due to their high toxicity and strong smell [2]. Chlorophenols remain in the environment and do long-term damage to environment and biology. The wastewater containing chlorophenols compounds has been suspected of carcinogenic and mutagenic effects on the living [3]. The reported level of chlorophenol concentration in wastewater is 0.1 mg L^{-1} according to the EPA and 0.001 mg L^{-1} in potable water according to the World Health Organization (WHO), respectively [4]. Chlorophenols cause a series of environmental and ecological problem as pollutants. Thus, it is crucial to develop more efficient technology to remove them from aqueous solutions.

At present, several chemical, physical and biological techniques, such as photocatalytic degradation [4], adsorption [5], chemical oxidation [6] and biological degradation [7], have been proposed for dealing with the chlorophenol-containing wastewater. Of all the methods, adsorption has been proved to be efficient and attractive in wastewater treatment [8]. In view of the traditional adsorption technology, it is hard to realize selective recognition of target molecule from environmental wastewater. Thus, aiming at efficient selective adsorption, it is highly desired to explore adsorbents that possess the properties of molecular recognition.

Molecular imprinting is an attractive technique for the preparation of three-dimensional polymeric materials with specific molecular recognition properties, namely molecular imprinting microspheres (MIS) [9]. MIS were obtained by polymerizing functional monomer and cross-linking monomer in the presence of the particular template molecular, which results in obtaining highly cross-linked microspheres matrix. After polymerization, the template molecular was removed from the polymeric matrix, leaving behind specific recognition site in MIS complementary to the template molecule in chemical functionality, size and geometry [10]. Due to properties such as high selectivity and affinity to the template molecule, MIS have been applied in many fields such as solid phase extraction [11], chromatography separation [12] and chemical sensing [13]. However, traditional MIS is still confronted with inherent limitations; they suffer the drawbacks of tedious filtration or centrifugation in the separation process.

†To whom correspondence should be addressed.
E-mail: jsdxtzj@126.com

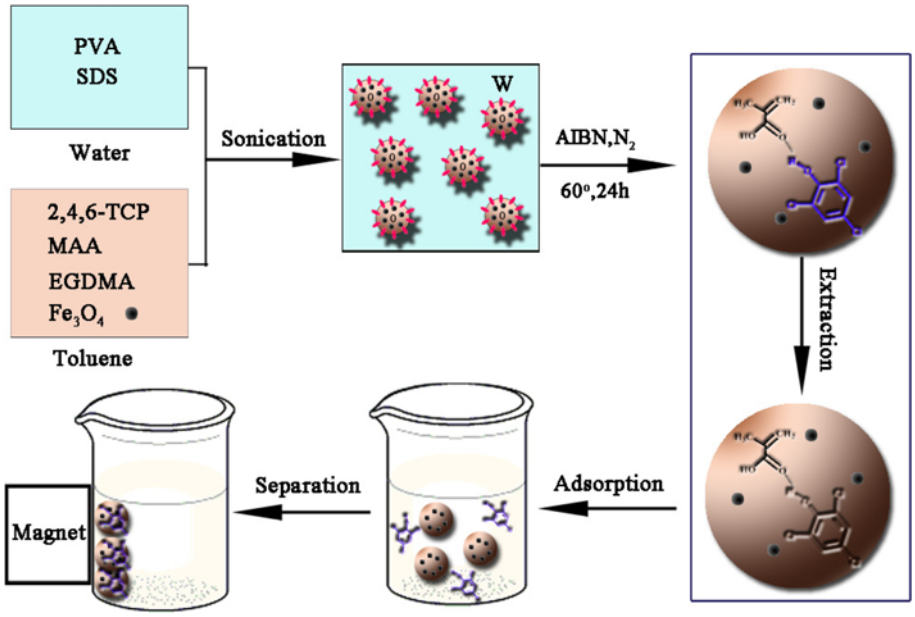

Fig. 1. Schematic route of magnetic molecular imprinting polymers prepared via suspension polymerization.

The drawbacks can be reduced by adopting a combination of conventional MIS and iron oxide magnetic nanoparticles. Magnetic molecularly imprinted microspheres (MMIS) not only have the advantage of magnetic response characters, but also have highly selective recognition characteristics to the template molecule. Recently, MMIS have received much more attention and have been applied in various fields [14,15]. A variety of MMIS have been prepared, including fast and selective determination of sulfonamides in honey based on MMIS [16], and selective enrichment of β-agonists in pork and pig liver samples based on MMIS [17]. The MMIS can use polymer-coated layer for selective recognition template molecule, and use magnetic materials to achieve rapid separation, instead of tedious filtration or centrifugation. In general, the synthesis methods of MMIS include bulk polymerization, precipitation polymerization, emulsion polymerization and suspension polymerization. Of all the methods, suspension polymerization has been confirmed to be the most efficient and powerful. Compared with the other methods, suspension polymerization exhibited good characteristics, such as the suspension polymerization system uses water as the continuous phase, the reaction temperature is easy to control, the cost is inexpensive and the purity of the products is quite high. It is concluded that MMIS synthesis by suspension polymerization could be the promising multifunctional adsorbent for the selective recognition target molecular.

Based on the above-mentioned work, our main purpose was to synthesize MMIS based on suspension polymerization, and then the MMIS was used for selective recognition of 2,4,6-TCP from aqueous solutions. The Fe_3O_4 nanoparticles synthesized by hydrothermal method were modified by oleic acid to improve hydrophobicity. Then the obtained acid-Fe_3O_4 nanoparticles were used as magnetic comonomer. The MMIS were synthesized by using 2,4,6-TCP as template molecule, methacrylic acid (MAA) as functional monomer, ethylene glycol dimethacrylate (EGDMA) as crosslinking, azodiisobutyronitrile (AIBN) as initiator, toluene as solvent, sodium dodecyl sulfate (SDS) as surfactant. The preparation of MMIS via suspension polymerization is illustrated in Fig. 1. The obtained MMIS were characterized by FT-IR, XRD, TGA, SEM and VSM. Adsorption equilibrium, kinetics and selectivity of the MMIS were investigated in detail. The MMIS were also used as adsorbents for the extraction of 2,4,6-TCP from the vegetable samples.

EXPERIMENTAL

1. Materials

Ferric trichloride ($FeCl_3 \cdot 6H_2O$), ethylene glycol, sodium acetate (NaAc), Azodiisobutyronitrile (AIBN) and Sodium dodecyl sulfate (SDS) were obtained from Aladdin Reagent Co., Ltd. (Shanghai, China). 2,4-dichlorophenol (2,4-DCP), 2,6-dichlorophenol (2,6-DCP), sesame phenol, thymol and 2,4,6-trichlorophenol (2,4,6-TCP) were purchased from Tianda Chemical Reagent Factory (Tianjin, China). Polyvinyl alcohol (PVA), methacrylic acid (MAA), oleic acid, acetic acid, dichloromethane, toluene, acetonitrile, ethanol and HPLC-grade methanol were obtained from Sinopharm Chemical Reagent Co., Ltd. (Shanghai, China). Ethyl glycol dimethacrylate (EGDMA) was obtained from Shanghai Xingtu Chemical Co., Ltd. (Shanghai, China). AIBN was recrystallized from methanol prior to use. Distilled water used in all experiments was purified with a Purelab Ultra (Organo, Tokyo, Japan). All other chemicals used were of analytical grade and obtained commercially.

2. Instruments and Apparatus

Infrared spectra (4,000-500 cm^{-1}) were recorded on a Nicolet NEXUS-470 FT-IR apparatus (USA). The morphology of the MMIS was observed by a scanning electron microscope (SEM, JEOL, JSM-7001F). Magnetic measurements were carried out using a vibrating sample magnetometer (VSM, 7300, Lakeshore) under a magnetic field up to 10 koe. Thermogravimetric analysis (TGA) was performed using a DSC/DTA-TG (STA 449C Jupiter, Netzsch, Germany) under a nitrogen atmosphere up to 800 °C with a heating

rate of 10 °C min^{-1}. The photographs of the magnetic separation were obtained by Canon IXUS125 HS. X-ray diffractometer (XRD) was carried out using a Rigaku D/max-γB over the 2θ range of 20-70° at a scanning rate of 7.0° min^{-1}. UV-vis adsorption spectra were obtained with a Unic-2602 UV-vis spectrophotometer (Unic Company, Shanghai, China), Other apparatus applied in this study are listed as follows: PHS-2 acidimeter (The Second Analytical Instrument Factory of Shanghai, China), Agilent1200 HPLC equipped with a UV-vis detector (Palo Alto, CA, USA), TG16-WS high-speed centrifuge (Changsha Xiangyi Centrifuge Factory, Province Jiangsu, China).

3. Preparation of Oleic Acid-modified Fe_3O_4 Magnetic Fluid

Fe_3O_4 nanoparticles were obtained according to our previous work [18]. First, 1.35 g of $FeCl_3 \cdot 6H_2O$ and 7.2 g sodium acetate were dispersed into the solution of ethylene glycol (40 mL) in a three-necked round-bottomed flask (100 mL) under nitrogen gas protection; with the purpose of obtaining a stable suspension, the mixture was stirred under nitrogen gas protection at 160 °C for 1.0 h. Then, the mixture was transferred into a 50-mL reaction flask and heated to 200 °C for 10.0 h, after the suspension was cooled to room temperature, washed with ethyl alcohol for three times and dried under vacuum at 60 °C, the Fe_3O_4 nanoparticles were obtained. Finally, 4 mL oleic acid was added to 0.1 g of Fe_3O_4 nanoparticles, the solution continued to be kept under stirring for another 1.0 h to obtain the magnetic fluid.

4. Synthetic of Magnetic Molecularly Imprinted Microspheres

Magnetic molecularly imprinted microspheres (MMIS) were synthetic by using a suspension polymerization method with few modifications [19]. As follows: First, 2,4,6-TCP (0.197 g) was dissolved in 5 mL of toluene, and 0.34 mL of MAA was dispersed into the mixture, which was stirred at room temperature for 30 min to obtain solution-1. AIBN (0.15 g), oleic acid-modified magnetic fluid (4 mL) was dissolved in a mixture of toluene (2 mL) and EGDMA (3.8 mL) to form solution-2. PVA (3.0 g) and distilled water (130 mL) was mixed together at 85 °C for 10 min, and then cooled to room temperature to form solution-3; SDS (1.0 g) was dispersed into distilled water (20 mL) to form solution-4. Then, solution-1 was combined with solution-2 while solution-3 and solution-4 were mixed together. The two mixtures were stirred separately for 2.0 h and then mixed together in a three-necked round-bottomed flask, purged with nitrogen for 10 min, and stirred at 600 rpm min^{-1} at room temperature for 1.0 h, and then the reaction was carried out with a stirring rate of 600 rpm min^{-1} at 60 °C for 24 h. Finally, the obtained microspheres were washed with ethanol and distilled water five times; the template molecules were washed with the mixture solution of methanol/acetic acid (90 : 10, v/v) using soxhlet extraction for 14 days. The prepared MMIS were washed with excess of distilled water until the pH of the solution equaled that of the distilled water. In comparison, the magnetic non-imprinted microspheres (MNIS) were also prepared with the same preparation method but without the addition of 2,4,6-TCP.

5. Batch Mode Binding Studies

The influences such as pH value, initial 2,4,6-TCP concentration, temperature, equilibration time and kinetics on the adsorption of 2,4,6-TCP from aqueous solutions were studied by a batch mode of experiments.

In study of pH value, 10 mL of solution containing 100 mg L^{-1} 2,4,6-TCP was reacted with the 10 mg of MMIS or MNIS. The solution initial pH value was adjusted from 2.0 to 8.0 by using 1 mol L^{-1} HCl and $NH_3 \cdot H_2O$ solutions. Then the solutions were stirred at constant temperature of 298 K for 12 h.

In the study of adsorption equilibrium, 10 mL of different initial concentration (from 10 to 400 mg L^{-1}) of 2,4,6-TCP solutions (pH=5) was contracted with 10 mg MMIS or MNIS. Then the mixture solutions were stirred at constant temperature of 298 K until the equilibrium was established.

In study of adsorption kinetics, 10 mL of solutions with different initial 2,4,6-TCP concentration (100 mg L^{-1} or 150 mg L^{-1}) (pH= 5) were mixed with 10 mg of MMIS or MNIS at different temperature (298 K or 308 K). Then the solutions were stirred for the desired time (10-480 min).

In study of regeneration, 10 mL of solutions with initial 2,4,6-TCP concentration 100 mg L^{-1} (pH=5) were mixed with 10 mg of MMIS or MNIS at constant temperature of 298 K for 12 h. After the desired time, the microspheres were magnetically separated. Subsequently, the mixture of methanol and acetic acid (10 : 90 V/V) was used as elution solutions and the microspheres were redissolved in 5.0 mL of elution solutions for 12 h. To investigate the regenerability of the MMIS, the adsorption and desorption cycles were repeated for five times.

After the desired time, the MMIS or MNIS were isolated from the solutions by Nd-Fe-B permanent magnet and the residual amount of 2,4,6-TCP in the aqueous phase was measured by UV-vis spectrophotometer at 290 nm.

The adsorption capacity of MMIS or MNIS (Q_e, mg g^{-1}) was calculated by the following equation:

$$Q_e = \frac{(C_0 - C_e)V}{W} \quad (1)$$

where C_0 (mg L^{-1}) and C_e (mg L^{-1}) represent the initial and equilibrium 2,4,6-TCP concentrations in the solution, respectively, V (mL) is the solution volume and W (mg) is the weight of the adsorbent.

6. Adsorption Selectivity

To investigate the selective recognition of 2,4,6-Tcp, 10 mg of MMIS or MNIS was added into 25 mL flasks, each of which contained 10 mL solution with 100 mg L^{-1} of 2,4,6-TCP, 2,4-DCP, 3-CP, sesame phenol and thymol, respectively. Moreover, the competitive adsorption of MMIS and MNIS for 2,4,6-TCP at the presence of 100 mg L^{-1} of 2,4-DCP, 3-CP, sesame phenol and thymol was studied. The pH of the initial solution was adjusted to 5.0 for both MMIS and MNIS, and the experiments were carried out on a thermostatic water bath at constant temperature of 298 K for 12 h.

7. Sample Preparation and SPE Procedure

Vegetable sample was prepared following our previous work [20]. Briefly, the edible parts of fresh cucumbers were squeezed into homogenates, and then 50 mL of acetonitrile was dumped into 50 g of scattered homogenate in an ultrasonic bath. After 6.0 h, the mixture was filtered and the filtrate was extracted with 30 mL of dichloromethane and evaporated to dryness using a rotary evaporator. Subsequently, the residue was redissolved in methanol, then appropriate amounts of 2,4,6-TCP were added into the water and vegetable samples mentioned above to form spiked samples, and the level of

spiked samples was 50 μg L^{-1}. The SPE process was according to the following steps: First, 30 mg of MMIS (or MNIS) was put into a beaker, then 5.0 mL of spiked samples was added into the beaker and the mixture was stirred for 3.0 h at 25 °C. Then the MMIS (or MNIS) with captured 2,4,6-TCP were separated from the solutions in the action of magnetic field. Subsequently, the MMIS (or MNIS) were washed with 4.0 mL of acetonitrile to reduce nonspecific adsorption. Finally, the 2,4,6-TCP templates molecule were eluted with 5.0 mL of methanol solution under the action of ultrasound and evaporated to dryness under nitrogen gas at 30 °C, then the residues were redissolved with 1.0 mL of 20% aqueous methanol for further high performance liquid chromatograph (HPLC) analysis. The injection loop volume was 30 μL, and the mobile phase consisted of 28% methanol and 72% deionized water, and the flow rate of the mobile phase was 1.0 mL min^{-1}.

RESULTS

1. Characterization of MMIS and MNIS

FT-IR spectra of Fe_3O_4 nanoparticles, MMIS and MNIS were determined with KBr pellet method and shown in Fig. 2. The main functional groups of the predicted structure can be observed with the corresponding infrared adsorption peaks [21]. The adsorption bonds around 569 and 633 cm^{-1} in Fe_3O_4 were attributed to the Fe-O groups [22], which were also obtained for MMIS and MNIS, Fig. 2 shows that the strength of Fe-O stretching decreased for both MMIS and MNIS, which was due to the coated polymer layer on the surface of the Fe_3O_4 nanoparticles. The results confirmed that Fe_3O_4 nanoparticles were introduced into MMIS and MNIS. The peaks around 1,732, 1,253 and 1,158 cm^{-1} of MMIS and MNIS were assigned to C=O stretching vibration of carboxyl (MAA), C-O symmetric and asymmetric stretching vibrations of ester (EGDMA), respectively [23]. The features around 2,856 and 2,927 cm^{-1} indicated CH_2 and CH_3 stretching vibration of MAA. All the above results indicated the presence of co-polymerization of MAA and EGDMA on the surface of polymer particles.

Fig. 3 shows the X-ray diffraction (XRD) patterns of MMIS and MNIS. It can be seen that the XRD patterns of MMIS and MNIS are similar, indicating both the imprinted and non-imprinted microspheres have the same composition. Moreover, in the 2θ range of 20-70°, six characteristic peaks that correspond to Fe_3O_4 (2θ=30.12, 35.47, 43.16, 53.52, 57.16, 62.69) were observed in the MMIS and MNIS, and the peak positions could be indexed to (2 2 0), (3 1 1), (4 0 0), (4 2 2), (5 1 1) and (4 4 0) (JCPDS card 19-0629 for Fe_3O_4) [23].

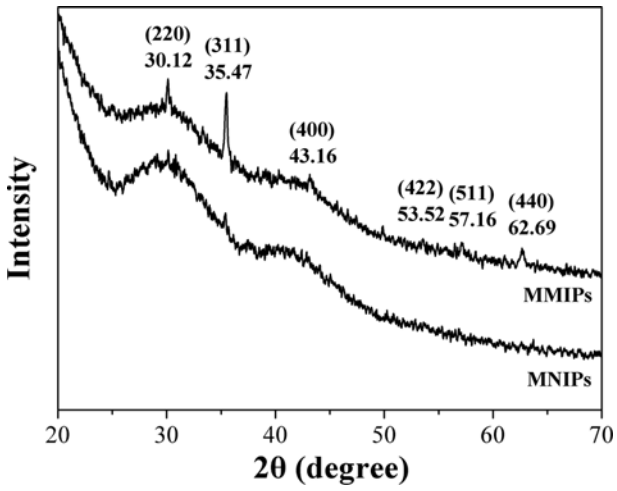

Fig. 3. XRD patterns of MMIS and MNIS.

The thermo-gravimetric analysis (TGA) curves of MMIS and MNIS are shown in Fig. 4. As can be seen, with the temperature range (<200 °C), MMIS and MNIS were difficult to be decomposed; the weight loss for MMIS and MNIS was mainly due to the evaporation of residual water. When the temperature increased to 420 °C, the TGA curve exhibited one significant weight loss for MMIS (83.61%) and MNIS (90.47%), respectively,; the reason was the rapid polymer decomposition. The weight loss of MMIS was different from that of MNIS, which might be attributed to the different degrees of polymerization, or residual imprinted 2,4,6-TCP. When the temperature finally rose above 450 °C, there was no weight loss and the remaining mass for MMIS and MNIS was attributed to the ther-

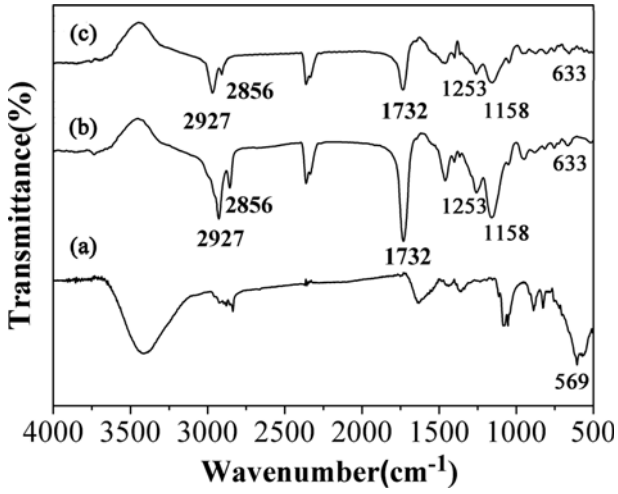

Fig. 2. FT-IR spectra of (a) Fe_3O_4 nanoparticles, (b) MMIS and (c) MNIS.

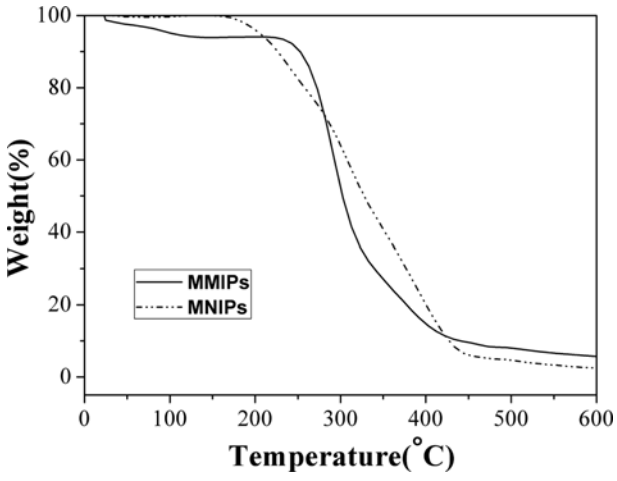

Fig. 4. TGA curves of MMIS and MNIS.

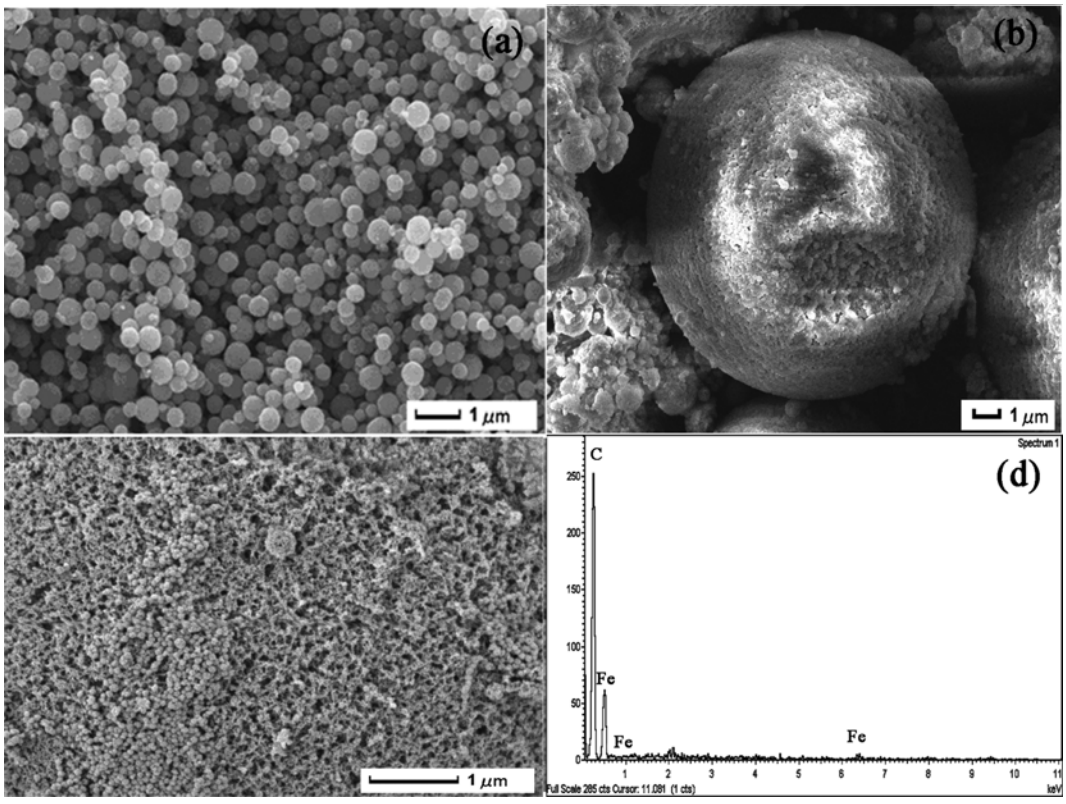

Fig. 5. SEM images of (a) Fe_3O_4 nanoparticles, (b) MMIS microspheres, (c) surface detail of MMIS and (d) energy spectrum diagram.

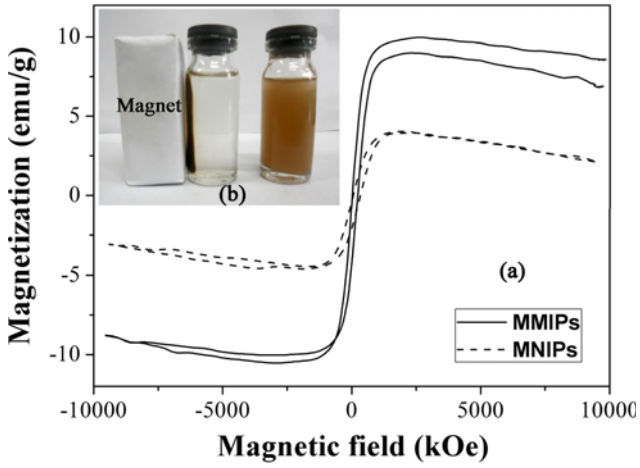

Fig. 6. Magnetization curves at room temperature of (a) MMIS and MNIS, (b) MMIS suspended in water (right) and separated by an external magnet (left).

mal resistance of iron particles and/or carbon particles.

The magnetic properties of MMIS and MNIS were applied by VSM. Fig. 6 shows the magnetic hysteresis loop of the two samples at room temperature. The similar shape of the two curves, being symmetrical about the origin, indicates that the microspheres were super paramagnetic [24]. The saturation magnetization (Ms) values were 10.14 emu g^{-1} and 4.2 emu g^{-1} for MMIS and MNIS, respectively. The theoretical specific saturation magnetization of bulk magnetite is reported to be 92 emu g^{-1} [25]. The decrease of magnetic intensity was mainly due to the small particle surface effect such as magnetically inactive layer containing spins that are not collinear with the magnetic field [26]. The adsorbents maintained enough magnetic to ensure the magnetic separation with the addition magnetic field. As can be seen from Fig. 6(b), it took about three minutes to attract the adsorbents from the brown dispersion with an extrinsic magnetic field.

2. Effect of Solution pH

Fig. 7 shows the adsorption performances of MMIS and MNIS for 2,4,6-TCP at different solution pH values. It is well known that optimization of pH value is a very important factor for adsorption. The pH of the solution affects the degree of ionization and that subsequently leads to a change in reaction kinetics and equilibrium characteristics of the adsorption process [27]. Fig. 7(a) shows that the adsorption capacity for MMIS and MNIS was approximately constant in the pH range of 2.0 to 6.0 and then reduced with increase the pH value from 6.0 to 8.0. It was probably because the pKa of MAA was about 5.80, when the pH>pKa values, MAA got deprotonated and then hydrogen bonds were disrupted between MAA and 2,4,6-TCP [28]. Moreover, the adsorption capacity achieved a maximum value at pH 6.0; the value was 72.75 mg g^{-1} for MMIS and 57.16 mg g^{-1} for MNIS, respectively. It is obvious that the adsorption capacity of MMIS was much higher than that of MNIS, strongly verifying the effect of imprinting. Thus, pH 6.0 for the adsorption medium was chosen for the following adsorption studies. Fig. 7(b) shows the effects of initial pH on final pH. There isn't significant change in pH value during the low pH 2.0 to 5.0. But with the increase of the pH value, the final pH was slightly lower

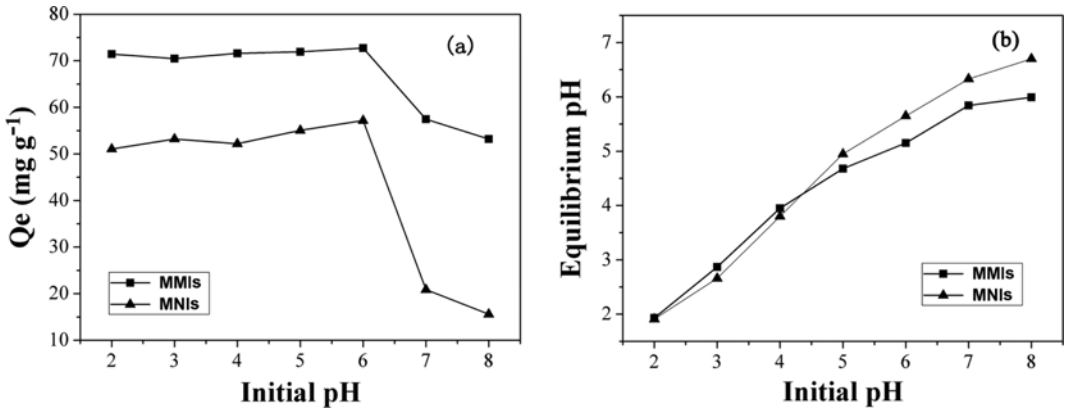

Fig. 7. (a) Effect of pH on adsorptive removal of 2,4,6-TCP and (b) effect of initial pH on equilibrium pH.

than the initial pH value. In previous studies, higher adsorption performance of phenolic compounds at lower pH value has also been reported by others [29,30]. The carboxyl groups and hydroxyl groups do not dissociate at lower pH value. With the increases of pH value, the dissociation degree of the carboxyl groups and hydroxyl groups is enhanced, resulting in the adsorption ability decline with the increase of pH value [31].

3. Adsorption Isotherm

The binding properties of MMIS and MNIS for 2,4,6-TCP were studied by the static adsorption experiments and the equilibrium data were fitted to the Langmuir [32] and Freundlich [33] adsorption isotherm models. The correlation coefficient (R^2) was used to judge the applicability of the isotherm models to the adsorption behaviors.

The linear and non-linear forms of the Langmuir isotherm models are expressed by the following equations, respectively:

$$\frac{C_e}{Q_e}=\frac{1}{Q_m K_L}+\frac{C_e}{Q_m} \tag{2}$$

$$Q_e=\frac{K_L Q_m C_e}{1+K_L C_e} \tag{3}$$

where C_e is the equilibrium concentration of adsorbate (mg L^{-1}), Q_m (mg g^{-1}) is the maximum adsorption capacity, Q_e is the equilibrium adsorption capacity (mg g^{-1}), K_L represents the affinity constant.

For predicting the favorability of an adsorption system, the Langmuir equation can also be expressed in terms of a dimensionless separation factor R_L [34].

$$R_L=\frac{1}{1+C_m K_L} \tag{4}$$

where C_m (mg L^{-1}) is the maximal initial 2,4,6-TCP concentration. The R_L value indicates whether the type of the isotherm is favorable ($0<R_L<1$), unfavorable ($R_L>1$), linear ($R_L=1$), or irreversible ($R_L=0$) [35].

The linear and non-linear form of the Freundlich isotherm models are expressed by the following equations, respectively:

$$\ln Q_e=\ln K_F+\left(\frac{1}{n}\right)\ln C_e \tag{5}$$

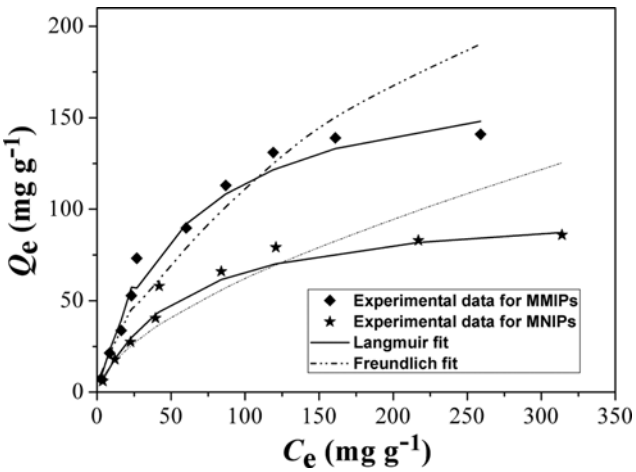

Fig. 8. Comparison of Langmuir and Freundlich isotherm models for 2,4,6-TCP adsorption onto MMIS and MNIS.

$$Q_e=K_F C_e^{1/n} \tag{6}$$

where K_F (mg g^{-1}) and n are the adsorption constants that indicate the adsorption capacity, the value of 1/n ranging from 0.1 to 1.0 represents a favorable adsorption condition.

Fig. 8 shows the regression curves of Langmuir and Freundlich isotherm models for MMIS and MNIS, and the adsorption isotherm constants at 298 K are listed in Table 1. As shown in Fig. 8,

Table 1. Adsorption isotherm constants for 2,4,6-TCP adsorption onto MMIS and MNIS

Adsorption isotherm models		MMIS	MNIS
Langmuir equation	R^2	0.9807	0.9877
	$Q_{m\text{-}c}$ (mg g^{-1})	181.82	103.11
	K_L (L mg^{-1})	0.0169	0.0176
	R_L	0.1285	0.124
Freundlich equation	R^2	0.9371	0.9064
	K_F (mg g^{-1})	5.1867	3.8321
	n	1.5008	1.6485

with increase of the initial concentration of 2,4,6-TCP from 10 mg L^{-1} to 400 mg L^{-1}, the adsorption capacity (Q_e) for MMIS and MNIS increased sharply, then increased slowly, and finally reached binding equilibrium, as expected. The maximum adsorption capacity (Q_e) for MMIS and MNIS at 298 K was 138.29 mg g^{-1} and 81.69 mg g^{-1}, respectively. The adsorption capacity of 2,4,6-TCP on MMIS was about 1.7 times higher than that of MMIS at the same conditions. The recognition sites on the surface and in the proximity of imprinted microspheres' surface displayed better steric matching with 2,4,6-TCP [36]. Moreover, these values were larger than microsphere studies by Pan's group [37]. By fitting the experimental data with Langmuir and Freundlich adsorption isotherm models, the fitted curves and correlation coefficient (R^2 values above 0.98) fully illustrated the Langmuir model fitted the experiment data better than the Freundlich model. The values of 1/n were less than 1.0 at 298 K, indicating that 2,4,6-TCP adsorption onto both MMIS and MNIS was favorable [38]. The results suggested the monolayer molecular adsorption for MNIS and multi-molecular layers adsorption for MMNIS [39].

4. Adsorption Kinetics

Pseudo first-order and pseudo second-order [40] models are commonly used in the literature to investigate the adsorption behavior of target molecules onto molecularly imprinted microspheres. The linear and non-linear forms of the pseudo-first-order model are expressed as follows:

$$\ln(Q_e - Q_t) = \ln Q_e - k_1 t \quad (7)$$

$$Q_t = Q_e - Q_e e^{-k_1 t} \quad (8)$$

The linear and non-linear forms of the pseudo-second-order model are expressed as follows:

$$\frac{t}{Q_t} = \frac{1}{K_2 Q_e^2} + \frac{t}{Q_e} \quad (9)$$

$$Q_t = \frac{k_2 Q_e^2 t}{1 + k_2 Q_e t} \quad (10)$$

where Q_t and Q_e (mg g^{-1}) are the amount adsorbed at various time t and equilibrium time, respectively. k_1 (min^{-1}), the equilibrium rate constant of the pseudo-first-order model can be obtained by plotting $\ln(Q_e - Q_t)$ versus t. k_2 (g mg^{-1} min^{-1}) is the pseudo-second-order model rate constant calculated from the plot of t/Q_t versus t. On the basis of pseudo-second-order model, the initial adsorption rate (h, mmol g^{-1} min^{-1}) and half-equilibrium time ($t_{1/2}$, min) were calculated according to the following equations:

$$h = K_2 Q_e^2 \quad (11)$$

$$t_{1/2} = \frac{1}{k_2 Q_e} \quad (12)$$

The adsorption kinetics constants and regression values at different initial concentrations of 2,4,6-TCP and temperatures are summarized in Table 2. The non-linear regression plots of pseudo-first-order model and pseudo-second-order model for 2,4,6-TCP binding onto MMIS and MNIS are shown in Fig. 9. The applicability

Table 2. Kinetic constants for the pseudo-first-order model and pseudo-second-order model

			Pseudo-first-order model				Pseudo-second-order model				
	C_0 (mg L^{-1})	T (K)	$Q_{e,exp}$ (mg g^{-1})	$Q_{e,c}$ (mg g^{-1})	k_1 (L min^{-1})	R^2	$Q_{e,c}$ (mg g^{-1})	k_2 (g mg^{-1} min^{-1})	R^2	h (mg g^{-1} min^{-1})	$t_{1/2}$ (min)
MMIS	100	298	73.51	26.17	0.0085	0.975	75.19	0.0008	0.999	4.52	16.62
	100	308	76.68	29.38	0.0081	0.98	78.13	0.00098	0.999	5.98	13.06
	150	298	88.95	31.07	0.0068	0.988	90.09	0.00073	0.999	5.95	15.14
MNIS	100	298	56.43	27.58	0.0078	0.967	58.48	0.00073	0.999	2.49	23.49
	100	308	59.89	32.27	0.0096	0.991	63.69	0.0007	0.998	2.85	22.38
	150	298	66.97	28.14	0.0069	0.956	68.49	0.00078	0.999	3.68	18.6

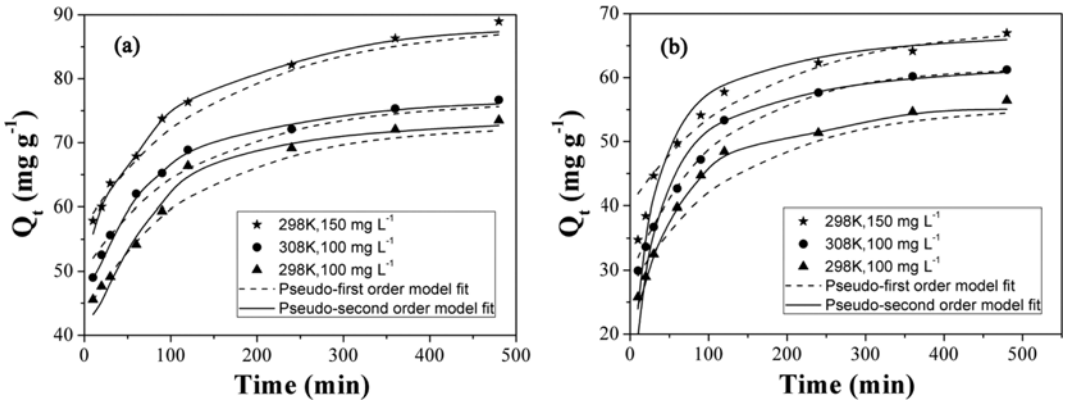

Fig. 9. Comparison of pseudo-first-order and pseudo-second-order kinetic models for 2,4,6-TCP adsorption onto (a) MMIS and (b) MNIS.

of the kinetic models to the adsorption process was studied by judging the correlation coefficient (R^2). Compared with the pseudo-first-order model, the pseudo-second-order model shows better results (R^2 values above 0.99) between the experimental values and theoretical values. The results suggest that the adsorption of 2,4,6-TCP onto MMIS and MNIS followed the pseudo-second-order model and the chemical process was the rate-limiting step in the adsorption process [42]. Table 2 illustrates that with the increase of temperature and initial concentration of 2,4,6-TCP, the adsorption capacity (Q_e) and the initial adsorption rate (h) increased obviously. The reason was that the initial concentrations of 2,4,6-TCP provided the necessary driving force to overcome the resistances of mass transfer between the solid phase and the aqueous phases [43]; and higher temperature was conducive for template molecules to pass the external boundary layer, and produced the enlargement of surface area [44]. Moreover, the adsorption capacity (Q_e) and initial adsorption rate (h) of the adsorption of 2,4,6-TCP onto MMIS was more than those of MNIS, indicating the presence of specific binding sites on the surface of MMIS.

5. Selectivity Study

To investigate the binding selectivity of the prepared MMIS for 2,4,6-TCP, reference phenol, such as sesamol, 3-CP, thymol and 2,4-DCP was selected. Fig. 10(a) shows the different molecular structures of all these reference phenol. Competitive phenol binding adsorption experiment were carried by adding 10 mg of MMIS and MNIS under the same condition, and the adsorbates were all at the same concentration of 100 mg L^{-1}. When it reached to the adsorption equilibrium, HPLC was used to determine the concentrations of each phenol.

Fig. 10(b) shows the binding capacity of the sesamol, 3-CP, thymol, 2,4-DCP and 2,4,6-TCP. It can be observed that MMIS exhibited higher binding capacity among the five phenols, indicating high binding selectivity for the template molecule (2,4,6-TCP). The reason was the imprinting effect; abundant binding sites were available for selective recognition 2,4,6-TCP. Fig. 10(b) clearly shows that the binding capacity for every phenol followed the order 2,4,6-TCP>2,4-DCP>3-CP>sesamol>thymol. The results could be attributed to the distinct molecular structure and functional groups of the phenols. Of all the phenols, sesamol and thymol molecules were too big to get into the imprinting cavities, although the molecular structure of 2,4-DCP and 3-CP was similar to the 2,4,6-TCP; and although the two phenols could easily get into the cavities imprinted by 2,4,6-TCP, the binding capacity of MMIS for 2,4,-DCP was still much lower than that of MMIS for 2,4,6-TCP, indicating the high selective recognition ability for 2,4,6-TCP.

To further testify to the specificity adsorption of MMIS for 2,4,6-TCP, four reference phenols (sesamol, 3-CP, thymol and 2,4-DCP) were added into 2,4,6-TCP solution, respectively, to form a binary solution with an initial concentration of 100 mg L^{-1}. 10 mg of MMIS or MNIS was dispersed into the binary solution to reach adsorption equilibrium. As shown in Fig. 10(c), MMIS still exhibited high adsorption capacity for 2,4,6-TCP in the presence of other competitive phenols, indicating higher selectivity adsorption in binary solution. The results confirmed the perfect imprinting effect in the polymerization.

6. Regeneration of MMIS and Sample Analysis

To inspect the regeneration performance of the MMIS, five regeneration cycles were conducted with 2,4,6-TCP. After adsorption, the mixture of acetic acid and methanol (10 : 90 v/v) was used as eluent solution. After a quick magnetic separation, MMIS were washed with 5.0 ml of elution solution for 12 h. The results are shown in Fig. 11; the adsorption capacities of MMIS for 2,4,6-TCP slightly decreased with increasing the using times. The rate of adsorption loss was calculated by the following formula:

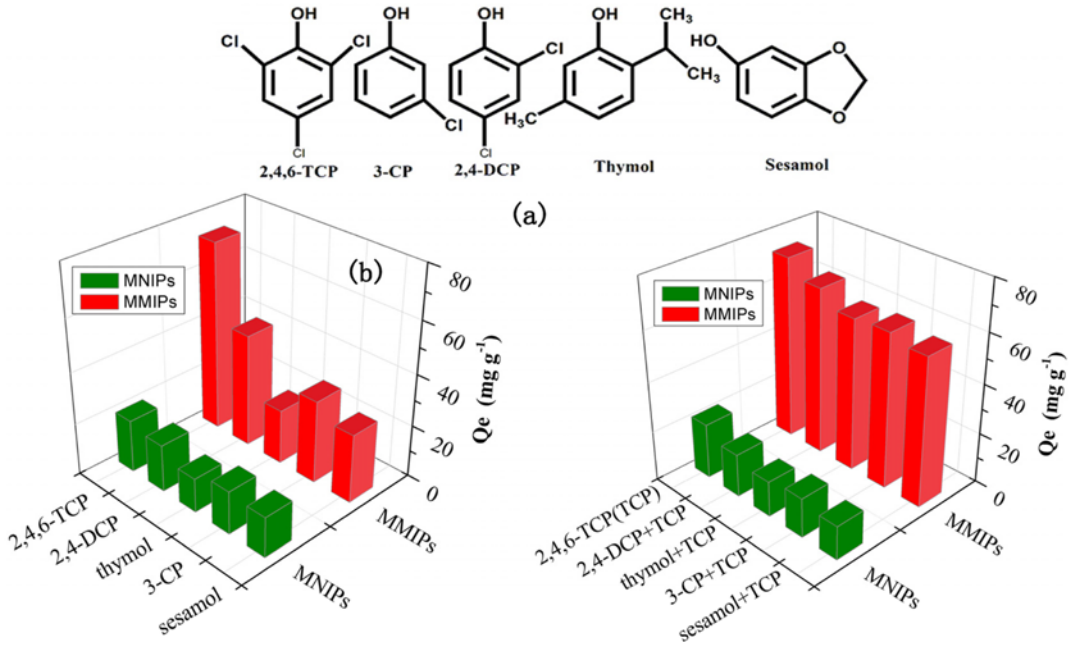

Fig. 10. Adsorption selectivity of 2,4,6-TCP onto MMIS and MNIS: (a) molecular structures of reference phenol, (b) single solution adsorption and (c) binary solution in the presence of reference phenol.

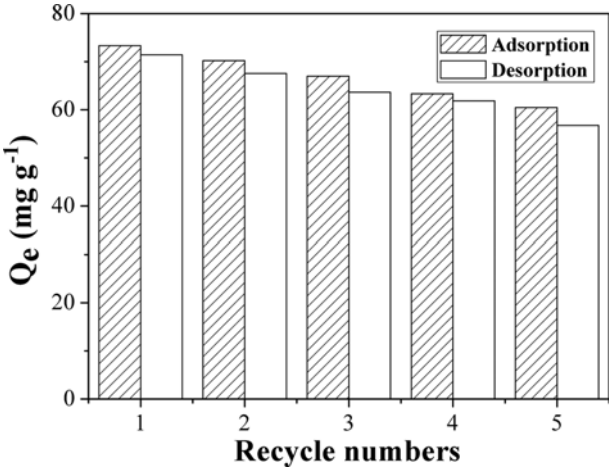

Fig. 11. Five recycles of regeneration at 298 K. methanol : acetic acid (V : V)=90 : 10 as eluent solution.

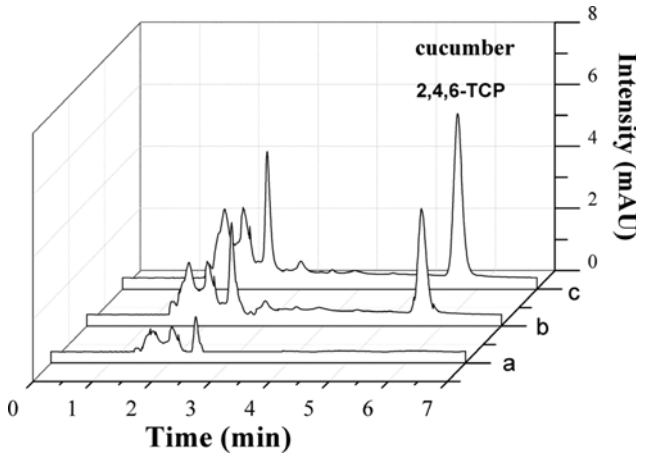

Fig. 12. HPLC chromatograms of spiked sample (a), extracted with MNIS (b) and MMIS (c).

$$R = \frac{(C_F - C_L)}{C_F} \quad (13)$$

where C_F is the adsorption capacity of the first time, and C_L is the adsorption capacity of the last time. The adsorption capacity of MMIS for 2,4,6-TCP was about 17.53% loss, indicating the renewable performance of MMIS.

To further validate the application of MMIS for the analysis of real samples, cucumber spiked with 2,4,6-TCP at 50 μg L^{-1} was analyzed, respectively, while MNIS were used for comparison. After the solid phase extraction, the chromatograms of spiked samples (a), MMIS (b) and MNIS (c) are shown in Fig. 12. From Fig. 12, it was very clear that no template molecule was detected in the spiked samples because the concentration of 2,4,6-TCP was quite low. But after the separation and enrichment of MMIS or MNIS, the chromatograms of spiked samples extraction by MMIS and MNIS exhibited peak of 2,4,6-TCP around 5.7 min, and the peak of MNIS was quite lower than that of MMIS under the same condition. The results illustrated that the MMIS showed a specific recognition ability for 2,4,6-TCP. Furthermore, the recovery of 84.37% was obtained for the cucumber spiked sample, Therefore, MMIS is suitable for trace analysis of 2,4,6-TCP in vegetable sample.

CONCLUSION

Novel magnetic molecularly imprinted microspheres were successfully synthesis-based on suspension polymerization and applied for selective recognition and removal of 2,4,6-TCP from aqueous solutions. The Fe_3O_4 nanoparticles were used as magnetic monomer participating in the polymerization process. Through a variety of characterization methods, the prepared MMIS exhibited good characteristics such as good thermal stability, magnetic property, excellent adsorption and specific recognition capacity. The MMIS can use polymer coated layer to selective recognition 2,4,6-TCP, and use Fe_3O_4 nanoparticles to achieve rapid separation. The adsorption and selective recognition ability were validated by a series of static adsorption experiments, with the results confirming that the prepared MMIS is capable of renewable and specificity adsorption target pollutants. We believe that MMIS is a powerful technique for environmental protection.

ACKNOWLEDGEMENTS

This work was financially supported by the National Natural Science Foundation of China (No. 21176107, No. 21107037), Research Fund for the Doctoral Program of Higher Education of China (No. 20110205110014), Jiangsu Planned Projects for Postdoctoral Research Funds (No. 1102119C), Siping Planned Projects for Development of Science and Technology (No. 2013043, No. 2012042), Natural Science Foundation of Jilin Province (No. 20130101179JC_15), Science and Technology Research Foundation of Jilin Province Department of Education (No. 2014_158)

REFERENCES

1. İ. Y. İpek, N. Kabay, M. Yüksel, D. Yapıcı and Ü. Yüksel, *Desalination*, **306**, 24 (2012).
2. V. C. Srivastava, M. M. Swamy, I. D. Mall, B. Prasad and I. M. Mishra, *Colloids Surf., A.*, **272**, 89 (2006).
3. J. A. Puhakka and K. Jarvinen, *Water Res.*, **26**, 765 (1992).
4. P. A. Deshpande and G. Madras, *Chem. Eng. J.*, **161**, 136 (2010).
5. Y. Li, X. Li, Y. Q. Li, J. Y. Qi, J. Bian and Y. X. Yuan, *Environ. Pollut.*, **157**, 1879 (2009).
6. Y. Liu, F. Wang, T. W. Tan and M. Lei, *Anal. Chim. Acta*, **581**, 137 (2007).
7. I. Gallizia, S. McClean and I. B. Banat, *J. Chem. Technol. Biot.*, **78**, 959 (2003).
8. G. H. Wu, Z. Q. Wang, J. Wang and C. Y. He, *Anal. Chim. Acta*, **582**, 304 (2007).
9. S. F. Xu, J. H. Li and L. X. Chen, *J. Mater. Chem.*, **21**, 4346 (2011).
10. G. Wulff, *Angew. Chem. Int. Ed.*, **34**, 1812 (1995).
11. X. M. Jiang, W. Tian, C. D. Zhao, H. X. Zhang and M. C. Liu, *Talanta*, **72**, 119 (2007).
12. R. Sancho and C. Minguillón, *Chem. Soc. Rev.*, **38**, 797 (2009).
13. L. M. Chang, Y. Li, J. Chu, J. Y. Qi and X. Li, *Anal. Chim. Acta*, **680**, 65 (2010).

14. G. Q. Pan, Q. P. Guo, Y. Ma, H. L. Yang and B. Li, *Angew. Chem. Int. Ed.*, **6907**, 52 (2013).
15. G. Q. Pan, Y. Zhang, Y. Ma, C. X. Li and H. Q. Zhang, *Angew. Chem. Int. Ed.*, **11731**, 50 (2011).
16. L. Chen, X. P. Zhang, L. Sun, Y. Xu, Q. L. Zeng, H. Wang, H. Y. Xu, H. Wang and L. Ding, *J. Agric. Food Chem.*, **57**, 10073 (2009).
17. Y. L. Hu, Y. W. Li, R. J. Liu, W. Tan and G. K. Li, *Talanta.*, **84**(2), 462 (2011).
18. P. Yu, Q. L. Sun, J. M. Pan and Z. J. Tan, *Adsorpt. Sci. Technol.*, **31**(7), 641 (2013).
19. H. Khan, T. Khan and J. K. Park, *Sep. Purif. Technol.*, **62**, 363 (2008).
20. J. M. Pan, W. Hu, X. H. Dai, W. Guan and Y. S. Yan, *J. Mater. Chem.*, **21**, 15741 (2011).
21. J. M. Pan, H. Yao, L. C. Xu, H. X. Ou and Y. S. Yan, *J. Phys. Chem. C.*, **115**, 5440 (2011).
22. K. Yoshimatsu, K. Reimhult, A. Krozer, K. Mosbach, K. Sode and L. Ye, *Anal. Chim. Acta*, **584**, 112 (2007).
23. H. Y. Zhu, R. Jiang, L. Xiao and W. Li, *J. Hazard. Mater.*, **179**, 251 (2010).
24. X. Wang, L. Y. Wang, X. W. He, Y. K. Zhang and L. X. Chen, *Talanta.*, **78**, 327 (2009).
25. V. S. Zaitsev, D. S. Filimonov, I. A. Presnyakov, R. J. Gambino and B. Chu, *J. Colloid Interface Sci.*, **212**, 49 (1999).
26. R. H. Kodama A. E. Berkowitz Jr., E. J. McNiff and S. Foner, *Phys. Rev. Lett.*, **77**, 394 (1996).
27. M. Sathishkumar, A. R. Binupriya, R. Selvakumar, K. K. Sheema, E. Yun and J. G. Choi, *J. Environ. Sci.*, **20**(9), 1046 (2008).
28. C. B. Liu, Z. L. Song, J. M. Pan, Y. S. Yan, Z. J. Cao, X. Wei, L. Gao, J. Wang, J. D. Dai and M. J. Meng, *Talanta 1*, **14**, 25 (2014).
29. M. Sathishkumar, A. R. Binupriya, D. Kavitha, R. Selvakumard, R. Jayabaland, J. G. Choi and S. E. Yun, *Chem. Eng. J.*, **147**, 265 (2009).
30. M. Sathishkumar, K. Vijayaraghavan, A. R. Binupriya, A. M. Stephan, J. G. Choi and S. E. Yun, J. *Colloid Interface Sci.*, **320**, 22 (2008).
31. F. Q. An, R. K. Du, X. H. Wang, M. Wan, X. Dai and J. F. Gao, *J. Hazard. Mater.*, **201**, 74 (2012).
32. M. Mazzotti, *J. Chromatogr. A.*, **1126**, 311 (2006).
33. S. J. Allen, G. Mckay and J. F. Porter, *J. Colloid Interface Sci.*, **280**, 322 (2004).
34. W. Zhang, L. Qin, X. W. He, W. Y. Li and Y. K. Zhang, *J. Chromatogr. A.*, **1216**, 4560 (2009).
35. X. X. Li, J. M. Pan, J. D. Dai, X. H. Dai, H. X. Ou and R. X. Zhang, *J. Sep. Sci.*, **35**, 2787 (2012).
36. J. D. Dai, J. M. Pan, L. C. Xu, X. X. Li and Y. S. Yan, *J. Hazard. Mater.*, **205**, 179 (2012).
37. J. M. Pan, H. Yao, X. X. Li, B. Wang, P. W. Huo, W. Z. Xu, H. X. Ou and Y. Y. Yan, *J. Hazard. Mater.*, **190**, 276 (2011).
38. C. P. Dwivedi, J. N. Sahu, C. R. Mohanty, B. R. Mohan and B. C. Meikap, *J. Hazard. Mater.*, **156**, 596 (2008).
39. X. X. Li, J. M. Pan, J. D. Dai, X. H. Dai and C. X. Li, *Chem. Eng. J.*, **198**, 503 (2012).
40. Y. S. Ho and G. McKay, *Process. Biochem.*, **34**, 451 (1999).
41. G. Baydemir, M. Andac, N. Bereli, R. Say and A. Denizli, *Ind. Eng. Chem. Res.*, **46**, 2843 (2007).
42. M. Mazzotti, *J. Chromatogr. A.*, **1126**, 311 (2006).
43. F. Q. An and B. J. Gao, *Desalination*, **249**, 1390 (2009).